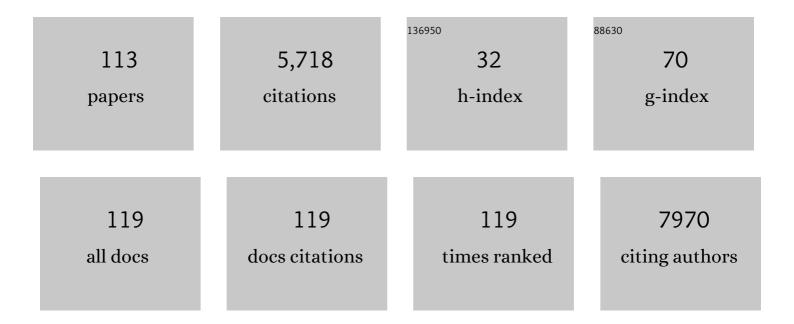
Michael A Chappell

List of Publications by Year in descending order

Source: https://exaly.com/author-pdf/8043974/publications.pdf Version: 2024-02-01



#	Article	IF	CITATIONS
1	Amide proton transfer imaging in stroke. NMR in Biomedicine, 2023, 36, e4734.	2.8	12
2	Validation of the estimation of the macrovascular contribution in multiâ€timepoint arterial spin labeling MRI using a 2â€component kinetic model. Magnetic Resonance in Medicine, 2022, 87, 85-101.	3.0	3
3	Quantitative chemical exchange saturation transfer imaging of nuclear overhauser effects in acute ischemic stroke. Magnetic Resonance in Medicine, 2022, , .	3.0	2
4	Review and consensus recommendations on clinical <scp>APT</scp> â€weighted imaging approaches at <scp>3T</scp> : Application to brain tumors. Magnetic Resonance in Medicine, 2022, 88, 546-574.	3.0	79
5	Study Protocol: The Heart and Brain Study. Frontiers in Physiology, 2021, 12, 643725.	2.8	2
6	Effect of Applying Leakage Correction on rCBV Measurement Derived From DSC-MRI in Enhancing and Nonenhancing Glioma. Frontiers in Oncology, 2021, 11, 648528.	2.8	9
7	Age-related normative changes in cerebral perfusion: Data from The Irish Longitudinal Study on Ageing (TILDA). NeuroImage, 2021, 229, 117741.	4.2	13
8	Examination of optimized protocols for pCASL: Sensitivity to macrovascular contamination, flow dispersion, and prolonged arterial transit time. Magnetic Resonance in Medicine, 2021, 86, 2208-2219.	3.0	8
9	Obesity is associated with reduced cerebral blood flow – modified by physical activity. Neurobiology of Aging, 2021, 105, 35-47.	3.1	31
10	Partial volume correction in arterial spin labeling perfusion MRI: A method to disentangle anatomy from physiology or an analysis step too far?. NeuroImage, 2021, 238, 118236.	4.2	33
11	Adapting the UK Biobank Brain Imaging Protocol and Analysis Pipeline for the C-MORE Multi-Organ Study of COVID-19 Survivors. Frontiers in Neurology, 2021, 12, 753284.	2.4	16
12	Robust Multi-TE ASL-Based Blood–Brain Barrier Integrity Measurements. Frontiers in Neuroscience, 2021, 15, 719676.	2.8	14
13	Imputing Biomarker Status from RWE Datasets—A Comparative Study. Journal of Personalized Medicine, 2021, 11, 1356.	2.5	1
14	Calibration of arterial spin labeling data—potential pitfalls in postâ€processing. Magnetic Resonance in Medicine, 2020, 83, 1222-1234.	3.0	36
15	Robust estimation of quantitative perfusion from multiâ€phase pseudoâ€continuous arterial spin labeling. Magnetic Resonance in Medicine, 2020, 83, 815-829.	3.0	1
16	Quantification of cerebral perfusion and cerebrovascular reserve using Turboâ€QUASAR arterial spin labeling MRI. Magnetic Resonance in Medicine, 2020, 83, 731-748.	3.0	11
17	Toblerone: Surface-Based Partial Volume Estimation. IEEE Transactions on Medical Imaging, 2020, 39, 1501-1510.	8.9	7
18	Designing and comparing optimized pseudo-continuous Arterial Spin Labeling protocols for measurement of cerebral blood flow. NeuroImage, 2020, 223, 117246.	4.2	19

#	Article	IF	CITATIONS
19	ExploreASL: An image processing pipeline for multi-center ASL perfusion MRI studies. NeuroImage, 2020, 219, 117031.	4.2	80
20	Does the magnetization transfer effect bias chemical exchange saturation transfer effects? Quantifying chemical exchange saturation transfer in the presence of magnetization transfer. Magnetic Resonance in Medicine, 2020, 84, 1359-1375.	3.0	3
21	Tumour subregion analysis of colorectal liver metastases using semi-automated clustering based on DCE-MRI: Comparison with histological subregions and impact on pharmacokinetic parameter analysis. European Journal of Radiology, 2020, 126, 108934.	2.6	5
22	Partial volume correction for quantitative CEST imaging of acute ischemic stroke. Magnetic Resonance in Medicine, 2019, 82, 1920-1928.	3.0	5
23	ICA-based denoising for ASL perfusion imaging. NeuroImage, 2019, 200, 363-372.	4.2	14
24	Model-based Bayesian inference of brain oxygenation using quantitative BOLD. NeuroImage, 2019, 202, 116106.	4.2	12
25	Tumor pH and Protein Concentration Contribute to the Signal of Amide Proton Transfer Magnetic Resonance Imaging. Cancer Research, 2019, 79, 1343-1352.	0.9	52
26	Association of Midlife Cardiovascular Risk Profiles With Cerebral Perfusion at Older Ages. JAMA Network Open, 2019, 2, e195776.	5.9	36
27	Measurement of collateral perfusion in acute stroke: a vessel-encoded arterial spin labeling study. Scientific Reports, 2019, 9, 8181.	3.3	19
28	Quantitative CEST imaging of amide proton transfer in acute ischaemic stroke. NeuroImage: Clinical, 2019, 23, 101833.	2.7	39
29	High temporal resolution arterial spin labeling MRI with wholeâ€brain coverage by combining timeâ€encoding with Look‣ocker and simultaneous multiâ€slice imaging. Magnetic Resonance in Medicine, 2019, 81, 3734-3744.	3.0	13
30	A general framework for optimizing arterial spin labeling MRI experiments. Magnetic Resonance in Medicine, 2019, 81, 2474-2488.	3.0	44
31	A framework for motion correction of background suppressed arterial spin labeling perfusion images acquired with simultaneous multiâ€slice EPI. Magnetic Resonance in Medicine, 2019, 81, 1553-1565.	3.0	2
32	Assessing Reliability of Myocardial Blood Flow After Motion Correction With Dynamic PET Using a Bayesian Framework. IEEE Transactions on Medical Imaging, 2019, 38, 1216-1226.	8.9	3
33	Visualizing arteryâ€specific blood flow patterns above the circle of Willis with vesselâ€encoded arterial spin labeling. Magnetic Resonance in Medicine, 2019, 81, 1595-1604.	3.0	12
34	The relationship between blood flow impairment and oxygen depletion in acute ischemic stroke imaged with magnetic resonance imaging. Journal of Cerebral Blood Flow and Metabolism, 2019, 39, 454-465.	4.3	10
35	Quantitative blood flow measurement in rat brain with multiphase arterial spin labelling magnetic resonance imaging. Journal of Cerebral Blood Flow and Metabolism, 2019, 39, 1557-1569.	4.3	33
36	4D-PET reconstruction using a spline-residue model with spatial and temporal roughness penalties. Physics in Medicine and Biology, 2018, 63, 095013.	3.0	4

1

#	Article	IF	CITATIONS
37	A DCE-MRI Driven 3-D Reaction-Diffusion Model of Solid Tumor Growth. IEEE Transactions on Medical Imaging, 2018, 37, 724-732.	8.9	37
38	Arterial spin labeling for the measurement of cerebral perfusion and angiography. Journal of Cerebral Blood Flow and Metabolism, 2018, 38, 603-626.	4.3	76
39	Enhancement of automated blood flow estimates (ENABLE) from arterial spin″abeled MRI. Journal of Magnetic Resonance Imaging, 2018, 47, 647-655.	3.4	30
40	Relationship between haemodynamic impairment and collateral blood flow in carotid artery disease. Journal of Cerebral Blood Flow and Metabolism, 2018, 38, 2021-2032.	4.3	48
41	Sensitivity of Multiphase Pseudocontinuous Arterial Spin Labelling (MP pCASL) Magnetic Resonance Imaging for Measuring Brain and Tumour Blood Flow in Mice. Contrast Media and Molecular Imaging, 2018, 2018, 1-11.	0.8	10
42	Extending the Human Connectome Project across ages: Imaging protocols for the Lifespan Development and Aging projects. NeuroImage, 2018, 183, 972-984.	4.2	290
43	Chemical exchange saturation transfer MRI shows low cerebral 2-deoxy-D-glucose uptake in a model of Alzheimer's Disease. Scientific Reports, 2018, 8, 9576.	3.3	33
44	Feasibility of Flat Panel Detector CT in Perfusion Assessment of Brain Arteriovenous Malformations: Initial Clinical Experience. American Journal of Neuroradiology, 2017, 38, 735-739.	2.4	4
45	A Variational Bayesian inference method for parametric imaging of PET data. Neurolmage, 2017, 150, 136-149.	4.2	23
46	Optimizing image registration and infarct definition in stroke research. Annals of Clinical and Translational Neurology, 2017, 4, 166-174.	3.7	17
47	A systematic study of the sensitivity of partial volume correction methods for the quantification of perfusion from pseudo-continuous arterial spin labeling MRI. NeuroImage, 2017, 162, 384-397.	4.2	37
48	A look-locker acquisition scheme for quantitative myocardial perfusion imaging with FAIR arterial spin labeling in humans at 3 tesla. Magnetic Resonance in Medicine, 2017, 78, 541-549.	3.0	11
49	4D-PET reconstruction of dynamic non-small cell lung cancer [18-F]-FMISO-PET data using adaptive-knot cubic B-splines. , 2017, , .		1
50	Quantification of Serial Cerebral Blood Flow in Acute Stroke Using Arterial Spin Labeling. Stroke, 2017, 48, 123-130.	2.0	28
51	Sub-Clinical Cognitive Decline and Resting Cerebral Blood Flow in Middle Aged Men. PLoS ONE, 2017, 12, e0169912.	2.5	7
52	Prospective motion correction and selective reacquisition using volumetric navigators for vesselâ€encoded arterial spin labeling dynamic angiography. Magnetic Resonance in Medicine, 2016, 76, 1420-1430.	3.0	13
53	Aerobic fitness is associated with greater hippocampal cerebral blood flow in children. Developmental Cognitive Neuroscience, 2016, 20, 52-58.	4.0	72

A DCE-MRI imaging-based model for simulation of vascular tumour growth. , 2016, 2016, 5949-5952.

#	Article	IF	CITATIONS
55	Determination of an optimally sensitive and specific chemical exchange saturation transfer MRI quantification metric in relevant biological phantoms. NMR in Biomedicine, 2016, 29, 1624-1633.	2.8	12
56	Tumor Growth Estimation via Registration of DCE-MRI Derived Tumor Specific Descriptors. , 2016, , .		0
57	Optimization of 4D vesselâ€selective arterial spin labeling angiography using balanced steadyâ€state free precession and vesselâ€encoding. NMR in Biomedicine, 2016, 29, 776-786.	2.8	31
58	Abstract 63: Novel Imaging of Protein Integrity to Better Define Ischemic Injury After Stroke. Stroke, 2016, 47, .	2.0	0
59	Automated removal of spurious intermediate cerebral blood flow volumes improves image quality among older patients: A clinical arterial spin labeling investigation. Journal of Magnetic Resonance Imaging, 2015, 42, 1377-1385.	3.4	35
60	Correcting for large vessel contamination in dynamic susceptibility contrast perfusion MRI by extension to a physiological model of the vasculature. Magnetic Resonance in Medicine, 2015, 74, 280-290.	3.0	6
61	Estimation of arterial arrival time and cerebral blood flow from QUASAR arterial spin labeling using stable spline. Magnetic Resonance in Medicine, 2015, 74, 1758-1767.	3.0	2
62	Patient-Specific Detection of Cerebral Blood Flow Alterations as Assessed by Arterial Spin Labeling in Drug-Resistant Epileptic Patients. PLoS ONE, 2015, 10, e0123975.	2.5	41
63	Quantification of errors in cerebral blood flow measurements due to dispersion in arterial spin labelling. , 2015, 2015, 7917-20.		1
64	Estimating the sample size required to detect an arterial spin labelling magnetic resonance imaging perfusion abnormality in voxel-wise group analyses. Journal of Neuroscience Methods, 2015, 245, 169-177.	2.5	9
65	Bayesian Model Inversion. , 2015, , 509-516.		0
66	Variational Bayes. , 2015, , 523-533.		1
67	Identifying the ischaemic penumbra using pH-weighted magnetic resonance imaging. Brain, 2015, 138, 36-42.	7.6	135
68	A Novel In Vivo Receptor Occupancy Methodology for the Glucocorticoid Receptor: Toward An Improved Understanding of Lung Pharmacokinetic/Pharmacodynamic Relationships. Journal of Pharmacology and Experimental Therapeutics, 2015, 353, 279-287.	2.5	15
69	Bolus Arrival Time and Cerebral Blood Flow Responses to Hypercarbia. Journal of Cerebral Blood Flow and Metabolism, 2014, 34, 1243-1252.	4.3	54
70	Optimization and Reliability of Multiple Postlabeling Delay Pseudo-Continuous Arterial Spin Labeling during Rest and Stimulus-Induced Functional Task Activation. Journal of Cerebral Blood Flow and Metabolism, 2014, 34, 1919-1927.	4.3	45
71	Comparing different analysis methods for quantifying the MRI amide proton transfer (APT) effect in hyperacute stroke patients. NMR in Biomedicine, 2014, 27, 1019-1029.	2.8	84
72	Validation of planningâ€free vesselâ€encoded pseudoâ€continuous arterial spin labeling MR imaging as territorialâ€ASL strategy by comparison to superâ€selective pâ€CASL MRI. Magnetic Resonance in Medicine, 2014, 71, 2059-2070.	3.0	16

#	Article	IF	CITATIONS
73	Quantification of amide proton transfer effect pre―and postâ€gadolinium contrast agent administration. Journal of Magnetic Resonance Imaging, 2014, 40, 832-838.	3.4	24
74	Modeling the residue function in DSCâ€MRI simulations: Analytical approximation to in vivo data. Magnetic Resonance in Medicine, 2014, 72, 1486-1491.	3.0	9
75	Modeling and correction of bolus dispersion effects in dynamic susceptibility contrast MRI. Magnetic Resonance in Medicine, 2014, 72, 1762-1774.	3.0	15
76	Effects of background suppression on the sensitivity of dual-echo arterial spin labeling MRI for BOLD and CBF signal changes. NeuroImage, 2014, 103, 316-322.	4.2	27
77	A New Similarity Metric for Groupwise Registration of Variable Flip Angle Sequences for Improved T 10 Estimation in DCE-MRI. Lecture Notes in Computer Science, 2014, , 154-163.	1.3	5
78	Modeling dispersion in arterial spin labeling: Validation using dynamic angiographic measurements. Magnetic Resonance in Medicine, 2013, 69, 563-570.	3.0	39
79	Comparing modelâ€based and modelâ€free analysis methods for QUASAR arterial spin labeling perfusion quantification. Magnetic Resonance in Medicine, 2013, 69, 1466-1475.	3.0	17
80	Pseudo-Continuous Arterial Spin Labelling MRI for Non-Invasive, Whole-Brain, Serial Quantification of Cerebral Blood Flow Following Aneurysmal Subarachnoid Haemorrhage. Translational Stroke Research, 2013, 4, 710-718.	4.2	8
81	Evaluating quantitative approaches to dynamic susceptibility contrast MRI among carotid endarterectomy patients. Journal of Magnetic Resonance Imaging, 2013, 37, 936-943.	3.4	8
82	A theoretical framework for quantifying blood volume flow rate from dynamic angiographic data and application to vessel-encoded arterial spin labeling MRI. Medical Image Analysis, 2013, 17, 1025-1036.	11.6	9
83	A control point interpolation method for the non-parametric quantification of cerebral haemodynamics from dynamic susceptibility contrast MRI. NeuroImage, 2013, 64, 560-570.	4.2	22
84	Quantitative Bayesian modelâ€based analysis of amide proton transfer MRI. Magnetic Resonance in Medicine, 2013, 70, 556-567.	3.0	51
85	Clinical Feasibility of Noninvasive Visualization of Lymphatic Flow with Principles of Spin Labeling MR Imaging: Implications for Lymphedema Assessment. Radiology, 2013, 269, 893-902.	7.3	40
86	Cerebral Blood Flow Quantification Using Vessel-Encoded Arterial Spin Labeling. Journal of Cerebral Blood Flow and Metabolism, 2013, 33, 1716-1724.	4.3	84
87	Optimal sampling schedule for chemical exchange saturation transfer. Magnetic Resonance in Medicine, 2013, 70, 1251-1262.	3.0	18
88	The Impact of Heterogeneity and Uncertainty on Prediction of Response to Therapy Using Dynamic MRI Data. Lecture Notes in Computer Science, 2013, 16, 316-323.	1.3	2
89	Quantitative measurement of cerebral physiology using respiratory-calibrated MRI. NeuroImage, 2012, 60, 582-591.	4.2	189
90	Evaluating the use of a continuous approximation for model-based quantification of pulsed chemical exchange saturation transfer (CEST). Journal of Magnetic Resonance, 2012, 222, 88-95.	2.1	29

#	Article	IF	CITATIONS
91	A kinetic model for vesselâ€encoded dynamic angiography with arterial spin labeling. Magnetic Resonance in Medicine, 2012, 68, 969-979.	3.0	26
92	A fast analysis method for non-invasive imaging of blood flow in individual cerebral arteries using vessel-encoded arterial spin labelling angiography. Medical Image Analysis, 2012, 16, 831-839.	11.6	25
93	Spontaneous blood oxygenation levelâ€dependent fMRI signal is modulated by behavioral state and correlates with evoked response in sensorimotor cortex: A 7.0â€T fMRI study. Human Brain Mapping, 2012, 33, 511-522.	3.6	20
94	Partial volume correction of multiple inversion time arterial spin labeling MRI data. Magnetic Resonance in Medicine, 2011, 65, 1173-1183.	3.0	133
95	Modelling of pH dynamics in brain cells after stroke. Interface Focus, 2011, 1, 408-416.	3.0	44
96	Intracranial Hemodynamics Is Altered by Carotid Artery Disease and After Endarterectomy. Stroke, 2011, 42, 979-984.	2.0	21
97	Assessment of arterial arrival times derived from multiple inversion time pulsed arterial spin labeling MRI. Magnetic Resonance in Medicine, 2010, 63, 641-647.	3.0	109
98	Separation of macrovascular signal in multiâ€inversion time arterial spin labelling MRI. Magnetic Resonance in Medicine, 2010, 63, 1357-1365.	3.0	101
99	Vesselâ€encoded dynamic magnetic resonance angiography using arterial spin labeling. Magnetic Resonance in Medicine, 2010, 64, 698-706.	3.0	43
100	A general framework for the analysis of vessel encoded arterial spin labeling for vascular territory mapping. Magnetic Resonance in Medicine, 2010, 64, 1529-1539.	3.0	34
101	Modelling the effects of cardiac pulsations in arterial spin labelling. Physics in Medicine and Biology, 2010, 55, 799-816.	3.0	5
102	Modeling the Effects of Flow Dispersion in Arterial Spin Labeling. IEEE Transactions on Biomedical Engineering, 2009, 56, 1635-1643.	4.2	16
103	Variational Bayesian Inference for a Nonlinear Forward Model. IEEE Transactions on Signal Processing, 2009, 57, 223-236.	5.3	333
104	Vascular Territory Image Analysis Using Vessel Encoded Arterial Spin Labeling. Lecture Notes in Computer Science, 2009, 12, 514-521.	1.3	2
105	Combined spatial and non-spatial prior for inference on MRI time-series. NeuroImage, 2009, 45, 795-809.	4.2	97
106	Bayesian analysis of neuroimaging data in FSL. NeuroImage, 2009, 45, S173-S186.	4.2	2,074
107	The effect of cavity geometry on the nucleation of bubbles from cavities. Journal of the Acoustical Society of America, 2007, 121, 853-862.	1.1	27
108	Modeling the Detachment and Transport of Bubbles From Nucleation Sites in Small Vessels. IEEE Transactions on Biomedical Engineering, 2007, 54, 2106-2108.	4.2	2

#	Article	IF	CITATIONS
109	Modeling the Cycles of Growth and Detachment of Bubbles in Carbonated Beverages. Journal of Physical Chemistry B, 2006, 110, 7579-7586.	2.6	27
110	A physiological model of gas pockets in crevices and their behavior under compression. Respiratory Physiology and Neurobiology, 2006, 152, 100-114.	1.6	12
111	A physiological model of the release of gas bubbles from crevices under decompression. Respiratory Physiology and Neurobiology, 2006, 153, 166-180.	1.6	28
112	A physiological model of the interaction between tissue bubbles and the formation of blood-borne bubbles under decompression. Physics in Medicine and Biology, 2006, 51, 2321-2338.	3.0	8
113	A Method for the Automated Detection of Venous Gas Bubbles in Humans Using Empirical Mode Decomposition. Annals of Biomedical Engineering, 2005, 33, 1411-1421.	2.5	16